Solar Physics
DOI: 10.1007/●●●●●-●●●-●●●-●●●●-●

Forward Modelling of Coronal Intensity Perturbations

I. De Moortel

S. J. Bradshaw

Abstract In this paper, forward modelling is used to investigate the relation between given temperature and density perturbations and the resulting (synthesised) intensity perturbations, as would be observed by e.g. TRACE and EIS (onboard Hinode). Complex and highly non-linear interactions between the components which make up the intensity (density, ionisation balance and emissivity) mean that it is non-trivial to reverse this process, i.e. obtain the density and temperature perturbations associated with observed intensity oscillations. In particular, it is found that the damping rate does not often 'survive' the forward modelling process, highlighting the need for a very careful interpretation of observed (intensity) damping rates. With a few examples, it is demonstrated that in some cases even the period of the oscillations can be altered and that it is possible for two different sets of input temperature and density to lead to very similar intensities (the well-known 'ill-posed' inversion process).

Keywords: MHD: oscillations - corona - activity

Received; Accepted

1. Introduction

Comparisons between theoretical models and observational data are crucial to enhancing our knowledge of the dynamic solar corona, both by guiding observations through theoretical predictions, as well as observationally constraining theoretical models (see e.g. Lundquist et al. (2004) who applied this idea to the elusive coronal heating mechanism). Most theoretical models will be expressed in terms of basic quantities such as temperature and density, which are not directly observable. Here, two different approaches are possible: forward modelling, where the theoretically predicted density and temperature are used to calculate the synthesised intensity, which can be directly compared to observed intensities.

School of Mathematics and Statistics, University of St Andrews, North Haugh, St Andrews, KY16 9SS, Scotland;
e-mail: ineke@mcs.st-and.ac.uk
Space and Atmospheric Physics Department, The Blackett Laboratory, Imperial College, London SW7 2BW, UK;
e-mail: s.bradshaw@imperial.ac.uk

The inverse approach is to try and extract estimates for temperature and density from observed intensities. However, as demonstrated by e.g. Wikstol, Judge and Hansteen (1998), Judge and McIntosh (1999) or McIntosh (2000), this inverse problem is often 'ill-posed' (see also Sect. 5 of the current manuscript) and the non-uniqueness of the solution has to be resolved by additional (implicit) information. Forward modelling also relies on extra assumptions but usually these are easier to control.

Generating observable quantities from theoretical models through forward modelling has been successfully demonstrated in the past by numerous authors. For example, the observational consequences of coronal heating by nanoflares has been studied extensively in a series of papers by Cargill and Klimchuk (Cargill 1993, 1994; Cargill and Klimchuk 1997; Klimchuk and Cargill 2001; Cargill and Klimchuk 2004). These authors investigate how different types of observables, such as broadband emission, spectroscopic information and differential emission measure, can (or cannot) contribute to our understanding of the nanoflare model. Numerical simulations carried out recently by Bradshaw and Cargill (2006) showed that blue-shifted emission associated with the nanoflare heating might be the most promising, observable signature of this heating mechanism. Similarly, Taroyan, Bradshaw and Doyle (2006) study the effect of nanoflare heating, synthesising the emission for a number of (mainly) transition region lines and found good agreement with the observed dynamical behaviour of these lines. These authors also suggest that the nanoflare scenario could be responsible for the average red-shifts often observed in transition region lines, which were studied previously by e.g. Hansteen (1993). Parenti et al. (2006) looked at the statistical properties of coronal loops, subject to turbulent heating and found significant changes in the power-law index of the synthesised emission compared with the input energy distribution. Also focussing on the coronal heating problem, Peter, Gudiksen and Nordlund (2004, 2006) looked at the synthesised emission spectra associated with heating through footpoint braiding, as simulated by Gudiksen and Nordlund (2005). A good (qualitative) agreement is found for the general appearance of the solar corona and, intriguingly, that the spatial variability in Doppler shifts in the corona is much stronger than the (spatial) variation in intensity, highlighting again the need to extend observational studies beyond intensity imaging alone.

Apart from coronal heating, several other dynamical processes occurring in the solar atmosphere have been studied using a forward modelling technique. For example, Innes and Tóth (1999) study explosive events in the chromospheric network by investigating the dynamical response of different emission lines to Petschek-like reconnection. The same events were modelled in more detail by Sarro et al. (1999), paying particular attention to the effects of non-equilibrium ionisation. Spectral signatures (Doppler shift and emission) of catastrophic cooling and downflows in coronal loops are examined by Müller, Peter and Hansteen (2004) and Müller et al. (2005), allowing a direct comparison with the observations of rapidly moving, localised brightenings ('blobs') in coronal loops by e.g. De Groof et al. (2004). Aiouaz, Peter and Keppens (2005) include the calculation of the Ne VIII line in their 2D model of coronal funnels. Different heating profiles lead to different Doppler shifts across the funnel, nicely illustrating how forward modelling can give us diagnostic tools to investigate the

physical processes occurring in the solar corona. Finally, we mention the work of Taroyan et al. (2007), who confirm the interpretation of loop oscillations, observed by SUMER/SOHO, as slow standing modes excited by microflare activity near a loop footpoint. In this study, the forward modelling allows the authors to shed light on the apparent absence of oscillations in intensity (as the hot loop oscillations have so far mainly been observed through variations in Doppler shifts).

The above summary of studies including forward modelling is by no means exhaustive but demonstrates that the approach has been successfully adopted by several authors, studying a variety of different phenomena in the solar atmosphere. However, forward modelling is by no means routinely included in comparisons between theoretical models and observational data. In this study, we use simple examples of damped intensity oscillations to demonstrate that one cannot assume that basic characteristics (e.g. damping rate) of the perturbations in the (input) temperature and density will necessarily be preserved in the synthesised emission. Although we are not aiming to model a specific physical or dynamical process, the study of decaying intensity oscillations is particularly relevant to the emerging field of coronal seismology (De Moortel, 2005; Nakariakov and Verwichte, 2005). The method we used is outlined in Section 2 and the effect on the damping rate and periodicity is demonstrated in Section 3 and 4, respectively. In Section 5, we briefly highlight the possible non-uniqueness of the solution again, before the discussion and conclusions in Section 6.

2. Forward Modelling Code

As we do not intend to investigate any particular damping mechanism, the temperature (T) and number density (n) we use as input for the forward modelling code are generated from simple analytical expressions. We will consider basic sinusoidal oscillations with an exponential damping profile, given by

$$T(s) = T_0 \left[1 + \delta T \, \sin\left(\frac{2\pi}{P}s + \phi_T\right) \exp(-\alpha s)\right], \quad (1)$$

$$n(s) = n_0 \left[1 + \delta n \, \sin\left(\frac{2\pi}{P}s + \phi_n\right) \exp(-\alpha s)\right], \quad (2)$$

where T_0 and n_0 represent the background temperature and density, respectively. Unless otherwise stated, we have set $n_0 = 10^9 \mathrm{cm}^{-3}$, $P = 20$, $\phi_n = \phi_T = 0$ and $\alpha = 0.5$. The coordinate s could represent either distance (e.g. along a coronal loop) or time. For the rest of this paper, we will assume that s represents the position along a loop, which will be denoted by z. However, we wish to emphasise here that our results with respect to spatial oscillations would equally apply to temporal oscillations. The perturbations in temperature (δT) and density (δn) are assumed to be related as

$$\delta n = \frac{\delta T}{\gamma - 1} = 1.5\,\delta T, \quad (3)$$

for $\gamma = 5/3$, where this relation has been derived from the ideal, 1D, adiabatic MHD equations.

To calculate the synthesised emission, we use the (equilibrium) ionisation balance as given by Mazzotta et al. (1998) and solar coronal abundances (which we assume to be constant) from Feldman et al. (1992). The ion emissivities were calculated using the atomic data package CHIANTI (Dere et al. 1997; Young et al. 2003). A look-up table in terms of $\log T$ and $\log n$ was created for the relevant ions, allowing the forward modelling code to just read the emissivities from this table, using basic linear interpolation. Using this information, the emission in units of DN cm^6 pixel^{-1}s^{-1} is given by

$$I(z) = \frac{0.83 \times A \times d \times B(T_e) \times R(\lambda) \times E(\lambda, n_e, T_e) \times \lambda}{n_e h c 4\pi}\,, \tag{4}$$

where the (electron) temperature and density are assumed to be functions of z (the position along the loop) and where 0.83 is the ratio of protons to electrons, A the abundance of the relevant ion relative to Hydrogen, d the line-of-sight depth, B the ionisation balance, R the appropriate instrument response function (obtained from SolarSoft), E the emissivity, h is Planck's constant and c is the speed of light. This quantity $I(z)$ is converted to intensity in units of DN pixel^{-1} s^{-1} by multiplying by n_e^2. The expression 'ionisation balance' of, for example, Fe IX is used as shorthand for the amount of Fe IX (as a fraction of the total amount of Fe) assuming ionisation equilibrium. For example, $B_{FeIX} = 0.3$ at $T = 10^6$ K means that, in ionisation equilibrium, 30% of Fe is in the Fe IX state at a temperature of 1 MK.

During the initial testing stages, the results from the forward modelling code were successfully compared to the forward modelling part of an already established code, HYDRAD (Bradshaw and Mason, 2003a, 2003b). To represent reasonable coronal loop values, we have (arbitrarily) assumed a line-of-sight depth of 5 Mm. We will focus our analysis on the TRACE 171 Å and 195 Å filters (Handy et al., 1999), and the EIS Fe XII (195.12 Å) emission line (Culhane et al., 2007). The TRACE emission is assumed to be well represented by the dominant emission lines, namely Fe IX and Fe X for the 171 Å filter and Fe VIII and Fe XII for the 195 Å filter.

2.1. Ionisation Equilibrium

If we assume s to represent a spatial coordinate, we can think of the type of perturbations defined in Equations. (1) and (2) as a model for driven, slow magnetoacoustic waves, propagating along a coronal loop. For coronal background temperatures, these waves will propagate at speeds of the order of 100-150 km s^{-1}. With an assumed wavelength of 20 Mm ($P = 20$), this results in a driving timescale of a few minutes. Our assumption of ionisation equilibrium will only be valid if these driving timescales are longer than the timescales it takes the relevant ions to reach ionisation equilibrium. To compute the relevant timescales, we numerically solve the full system of coupled differential equations which govern the ionisation balance, using a modified version of HYDRAD (Bradshaw

Table 1. An overview of the timescales for the Fe X and Fe XII ion populations to return to within 1% of ionisation equilibrium after the plasma is heated from 1 MK to 1.1 MK (for Fe X) and 1.5 to 1.65 MK (for Fe XII) for a range of perturbation timescales (τ) and densities. If there is no number, the maximum deviation from equilibrium is always smaller than 1%. The percentage between brackets is the *maximum* deviation from equilibrium during the heating phase for each case.

	Fe X			Fe XII		
Density (cm^{-3}) / Pert. time	1×10^9	2×10^9	5×10^9	1×10^9	2×10^9	5×10^9
$\tau = 0.1$ s	45 s (14.5%)	23 s (14.5%)	10 s (14.5%)	80 s (15.2%)	40 s (15.2%)	16 s (15.2%)
$\tau = 10.0$ s	40 s (13.5%)	18 s (11.5%)	6 s (6%)	75 s (14.5%)	35 s (13%)	13 s (8.5%)
$\tau = 60.0$ s	25 s (5.2%)	5 s (2.7%)	2 s (1.1%)	55 s (7.5%)	22 s (4.5%)	8 s (2.0%)
$\tau = 120.0$ s	15 s (2.7%)	5 s (1.4%)	- (0.6%)	40 s (4.5%)	15 s (2.5%)	1 s (1.1%)
$\tau = 300.0$ s	5 s (1.1%)	- (0.6%)	- (0.2%)	20 s (2.0%)	2 s (1.1%)	- (0.5%)

and Mason, 2003a, 2003b). Starting from initial temperatures $T_i = 1$ MK (for Fe X) and 1.5 MK (for Fe XII), the plasma temperature is raised to $T_f = 1.1$ MK (Fe X) and 1.65 MK (Fe XII), i.e. a 10% perturbation, on timescales of τ= 0.1, 10.0, 60.0, 120.0 and 300.0 seconds. Once T_f is reached, the plasma temperature is held fixed and the time it takes the ionisation balance to equilibrate is noted. The ion population is assumed to have reached equilibrium if it is within 1% of its equilibrium value at the higher temperature T_f. Table 1 gives an overview of this timescale for both the Fe X and Fe XII populations, for a range of different values of τ and density. It is clear that for typical coronal densities, i.e. $n \geq 10^9$ cm^{-3}, the Fe X and Fe XII populations can be assumed to have reached ionisation equilibrium on a timescale of the order of tens of seconds or less. Furthermore, the maximum deviation from ionisation equilibrium (percentages between brackets) is never more than about 15%. The physical situation we will study in this paper corresponds to a heating timescale of order minutes, for which the timescale for the ion balance to equilibrate is of order seconds. Hence, ionisation equilibrium is a reasonable assumption for our study and it will be a good proxy for temperature variations. We remind the reader again that the perturbations could equally represent spatial or temporal, standing oscillations with periodicities of a few minutes.

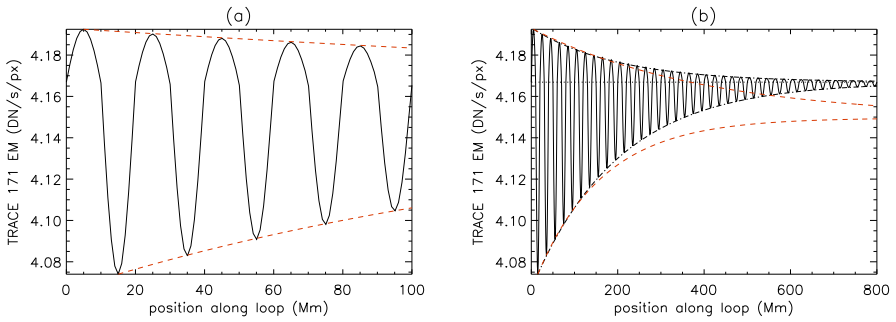

Figure 1. (a) TRACE 171 Å synthesised emission limited to the first 100 Mm along the loop and estimated damping profiles (dashed lines) for a background temperature $T_0 = 1$ MK and a 1% perturbation ($\delta T = 0.01$). (b) The same TRACE 171 Å synthesised emission and (dot-dashed lines) original (i.e. the input $e^{-\alpha z}$ profile) and (dashed lines) fitted (i.e. estimated from the first 100 Mm) damping profiles. The horizontal dotted line represents the background TRACE 171 Å emission.

3. Effect on Damping Rates

3.1. TRACE 171 Å Intensity

In this section, we investigate whether the chosen damping rate (α) 'survives' the forward modelling. This will have important implications for the interpretation of observed damping of periodic intensity perturbations (which could be either spatial or temporal damping). Indeed, when trying to identify the dominant damping mechanism on the basis of an observed (intensity) decay rate, it is essential to know if there is indeed a one-to-one relationship between the 'input' temperature and density perturbations and the resulting intensity perturbation. Additionally, we usually only observe a few cycles of periodic disturbances before the signal decays or deteriorates too much to be observed. Hence, we will base our estimates of the damping rate on the first few wavelengths along the loop.

Figure 1 shows the synthesised TRACE 171 Å intensity perturbations, resulting from a 1% temperature perturbation ($\delta T = 0.01$) around a background temperature of $T_0 = 10^6$ K. Figure 1 (a) only shows the first 100 Mm along the loop and overplotted are the exponential damping profiles ($\sim e^{-\alpha_{obs} z}$) obtained by matching the intensity maxima and minima (dashed lines) over this section. For the maxima, we obtain a damping coefficient of $\alpha_{obs} = 0.5\alpha$, whereas for the minima, we find $\alpha_{obs} = 1.3\alpha$. Clearly, these 'observed' values differ significantly from the original input damping rate. When we compare this to Figure 1 (b), where the same TRACE 171 Å intensity is shown for a much larger distance (800 Mm), it is clear that these damping profiles estimated from the first few peaks (dashed lines) are only a good match in this initial region but deviate substantially from the actual intensity at larger distances.

Comparing Figures 1 (a) and (b) we can see that the main reason for the error in our 'observed' damping profiles is the fact that they tend to the wrong background value at large distances. Looking at Figure 1 (b) it is clear that this background value (horizontal dotted line) is hard to estimate in the lower part

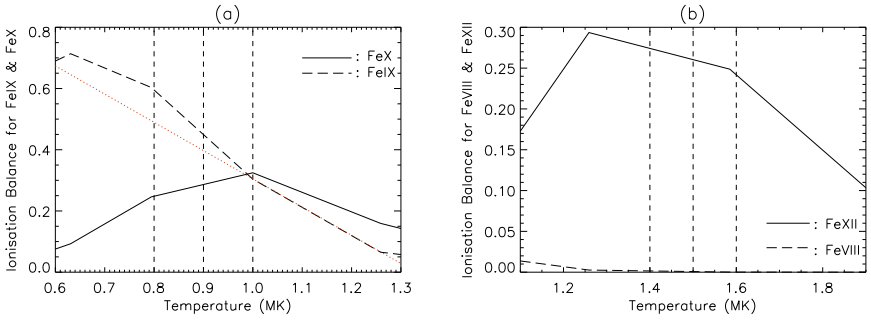

Figure 2. (a) The ionisation balance for Fe IX (long dashed line) and Fe X (solid line). The vertical dashed lines indicate $T_0 = 0.8$ MK, $T_0 = 0.9$ MK and $T_0 = 1$ MK. The dotted line represents a linear fit to the Fe IX ionisation balance just above $T_0 = 1$ MK. (b) The ionisation balance for Fe VIII (long dashed line) and Fe XII (solid line). The vertical dashed lines correspond to $T_0 = 1.4$ MK, $T_0 = 1.5$ MK and $T_0 = 1.6$ MK.

of the loop due to the very asymmetrical nature of the intensity perturbations. This asymmetry is mainly due to the suppression of the Fe X positive peaks, plus a (slight) enhancement of the negative peaks, caused by the nature of the Fe X ionisation balance around $T_0 = 10^6$ K. Indeed, the peak of the Fe X ionisation balance occurs exactly at 1 MK so regardless of whether the temperature perturbations are positive or negative, the ionisation balance will be decreasing compared to the background value (see Figure 2a). We will discuss this asymmetric nature in more detail below. Obviously, in these simple analytical examples the background value is exactly the same as the intensity at $z = 0$ but, as this is unlikely to be easily identified in real observations, we will not rely on this value. If the background value around which the perturbations are oscillating is known, the correct damping rate can be recovered (black dot-dashed lines). However, we will see later that even this is not always the case. Obviously, an 800 Mm coronal loop length is somewhat unrealistic but Figure 1 (b) really only serves to illustrate the fact that the estimated damping profile will tend to the wrong asymptotic value. In practise, the 100 Mm section we are using to estimate the damping profile is likely to be a significant fraction of the total loop length. Furthermore, the most important aspect is not the actual lengthscales, but the number of cycles of the periodic disturbance that can be reliably used to estimate the damping rate.

Table 2 provides an overview of the factors by which the 'observed' damping rates (i.e. the damping rates obtained from fitting the synthesised intensity extrema over the first 100 Mm along the loop) differ from the original value of the damping coefficient α for a range of background temperatures and temperature (and corresponding density) perturbations. Focussing on the TRACE 171 Å intensity, it is clear that the correct damping rate is only recovered in a few cases and that different amplitudes lead to different changes in the damping rate. In other words, the intensity perturbations do *not* just scale linearly, due to the non-linear interactions between the density, the instrument response function and the ionisation balance and emissivity of Fe IX and Fe X. We will try to

Table 2. Overview of the damping rates obtained from the synthesised emissions, as fractions of the original damping rate. For each value of the temperature perturbation δT, the top row is the damping rate estimated from fitting the maxima of the synthesised emission, whereas the bottom row corresponds to the damping rate obtained from the minima. $^{(a)}$In this case, a different damping profile of $e^{-0.6\alpha z^3}$ was obtained. $^{(b)}$ Damping profile of $e^{-\alpha z^2}$. $^{(c)}$ Intensity oscillations are out of phase with the original temperature and density perturbations.

	TRACE 171 Å			TRACE 195 Å			EIS Fe XII (195.12 Å)		
T_0 *(MK)*	0.8	0.9	1.0	1.4	1.5	1.6	1.4	1.5	1.6
δT=1%	1.0	1.0	0.5	1.0	1.0	0.75$^{(c)}$	1.0	1.0	0.75$^{(c)}$
	1.25	0.95	1.3	1.0	0.95	1.15$^{(c)}$	1.0	0.95	1.15$^{(c)}$
δT=5%	0.9	1.05	0.25	1.0	1.0	0.0	1.0	1.0	0.0
	1.1	0.95	1.3	0.95	0.95	2.3	0.95	0.95	2.3
δT=10%	0.95	1.05	0.0	1.0	0.0	0.0	1.0	0.0	0.0
	0.95	0.95	1.3	0.95	1.0	2.0	0.95	1.0	2.0
δT=15%	0.9	0.6$^{(a)}$	0.0	1.0$^{(b)}$	-0.2	0.0	1.0$^{(b)}$	-0.2	0.0
	0.9	1.1	1.3	1.65	1.1	2.0	1.65	1.1	2.0

disentangle this complex interplay for one particular example in detail, namely $T_0 = 10^6$ K, but a similar line of reasoning can be applied to each of the examples.

Figure 3 (a) shows the synthesised TRACE 171 Å emission resulting from perturbations in temperature and density around a background temperature $T_0 = 10^6$ K and density $n_0 = 10^9$ cm^{-3}. The various colours represent different (temperature) perturbations: black=1%, green=5%, blue=10% and red=15%. Two things are immediately obvious. Firstly, the emitted intensity is extremely asymmetric, with the minima being much more pronounced than the corresponding maxima, especially for the larger perturbations. Secondly, we can now see clearly that the intensity perturbations do not just scale linearly, i.e. the 15% perturbation is not just 15 times larger than the 1% perturbation. This is especially clear when looking at the maxima, where the 15% maxima even start to 'dip'. To understand the behaviour of the emitted TRACE 171 Å intensity, we look at the two components which make up this emission, namely the Fe IX and Fe X emission, shown in Figure 3 (b). As expected, given the relatively large background temperature ($T_0 = 10^6$ K), the TRACE 171 Å intensity is dominated by the Fe X emission (solid lines), which exhibits a similar asymmetry. However, the contribution of Fe IX (long-dashed lines) is not negligible and it is in fact the addition of the 'negative' maxima of Fe IX which causes the dips in the maxima of the 15% TRACE intensity. Indeed, the Fe IX emission exhibits an inverse behaviour, with the Fe IX emission decreasing when the temperature and density perturbations are actually increasing. Comparing Figures 3 (a) and (b), it is relatively straightforward to see how the behaviour of the synthesised TRACE 171 Å emission can be explained in terms of the individual Fe IX and Fe X emission. In the next two sections, we will focus firstly on the non-linear beha-

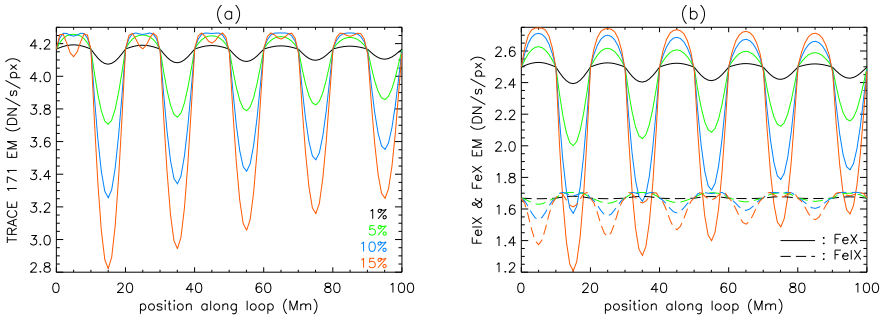

Figure 3. (a) TRACE 171 Å synthesised emission for a background temperature $T_0 = 1$ MK and a 1% (black), 5% (green), 10% (blue) and 15% (red) temperature perturbation. (b) The corresponding Fe IX (long dashed lines) and Fe X (solid lines) intensities which make up the TRACE 171 Å synthesised emission shown in Figure 3 (a).

viour of the Fe IX and Fe X emission and secondly, on the individual components of the emission, in particular the ionisation balance and the emissivity.

3.1.1. Non-linearity

As seen in Figure 3 (b), the Fe IX and Fe X emission around $T_0 = 1$ MK do not scale linearly. However, as we are using a linear interpolation to determine the values of the ionisation balance and emissivity, these quantities will behave linearly, as long as no change in gradient in the ionisation balance (B) or emissivity (E) is encountered. In other words, if we look at a Taylor expansion of, say, the ionisation balance,

$$B(T_0 + \delta T) = B(T_0) + \delta T \left.\frac{dB}{dT}\right|_{T=T_0} + O(\delta T^2), \tag{5}$$

we can limit this expansion to first order terms. Hence, the ionisation balance and (similarly) the emissivity can be written as

$$B \sim B_0(1 + c\delta T) \qquad \text{and} \qquad E \sim E_0(1 + a\delta n + b\delta T)\,, \tag{6}$$

with $E_0 = E(T_0, n_0)$ and $B_0 = B(T_0)$, and where

$$a = E_0^{-1} \left.\frac{\partial E}{\partial n}\right|_{n=n_0, T=T_0}$$
$$b = E_0^{-1} \left.\frac{\partial E}{\partial T}\right|_{T=T_0, n=n_0}$$
$$c = B_0^{-1} \left.\frac{dB}{dT}\right|_{T=T_0}.$$

So if the individual components scale linearly, why is the corresponding emission highly non-linear? As the non-linearity is most pronounced for Fe IX, let

us look at this case in more detail. As in Equation 4, we can write the Fe IX emission as

$$I_{FeIX}(T_0+\delta T, n_0+\delta n) = B(T_0+\delta T)\times E(T_0+\delta T, n_0+\delta n)\times n^2(n_0+\delta n)\,, \quad (7)$$

where, for convenience of notation, we have absorbed all the constants (i.e. terms which do not depend on z) present in Equation 4 into the emissivity E. Using the (linear) Taylor expansions given in Equation 6, we can rewrite this as

$$I_{FeIX} = n_0^2(1+\delta n)^2 \times B_0(1+c\delta T)\times E_0(1+a\delta n + b\delta T)\,.$$

Remembering that we are using the relation $\delta n = \delta T/(\gamma-1)$, we find

$$I_{FeIX} \sim 1 + \beta_1\delta T + \beta_2\delta T^2 + O(\delta T^3)\,,$$

where

$$\begin{aligned}\beta_1 &= c + \frac{a}{\gamma-1} + b + \frac{2}{\gamma-1}\,,\\ \beta_2 &= c\left(\frac{a}{\gamma-1}+b\right) + \frac{2}{\gamma-1}\left(\frac{a}{\gamma-1}+b+c\right) + \frac{1}{(\gamma-1)^2}\,.\end{aligned}$$

The Fe IX intensity will only behave linearly when we can ignore the higher order terms, i.e. when $\delta T \ll \beta_1/\beta_2$. From a linear fit to the Fe IX ionisation balance just above $T_0 = 10^6$ K (see Figure 2a - dotted line), we find a gradient $c = -3.02$. Similarly, for the Fe IX emissivity, we find gradients $a = 0$ and $b = 0.24$. Substituting these values in the above expressions for β_1 and β_2, we find $\beta_1/\beta_2 = 0.032$, implying that the higher order terms can only be ignored for $\delta T \ll 3\%$. Hence, it becomes clear that for the examples we are considering ($\delta T = 1\% - 15\%$), the Fe IX emission will not scale linearly, despite the fact that its individual components do behave linearly (around $T_0 = 10^6$ K).

3.1.2. Ionisation Balance and Emissivity

To gain a deeper understanding of the Fe IX and Fe X emission, we will now focus on the two main building blocks (see Equation 4) of the respective Fe emissions, namely the ionisation balance and the emissivity of Fe IX and Fe X. As it is the dominant component, let us start with the Fe X emission. Figure 4 shows (a) the ionisation balance and (b) the integrated (over all relevant wavelengths) emissivity of both Fe IX (long-dashed) and Fe X (solid). Note that, as the emissivity has been summed over all wavelengths, the effect of the instrument response function is essentially folded in to E. The various colours represent the same perturbation amplitudes as above but scaled to the 15% perturbation (e.g. the 1% perturbation has been increased by a factor of 15, etc). This scaling was carried out to confirm that both the ionisation balance and the emissivity do indeed behave largely linearly around $T_0 = 1.0$ MK (providing further justification of the linear approximation to B and E made in the previous section).

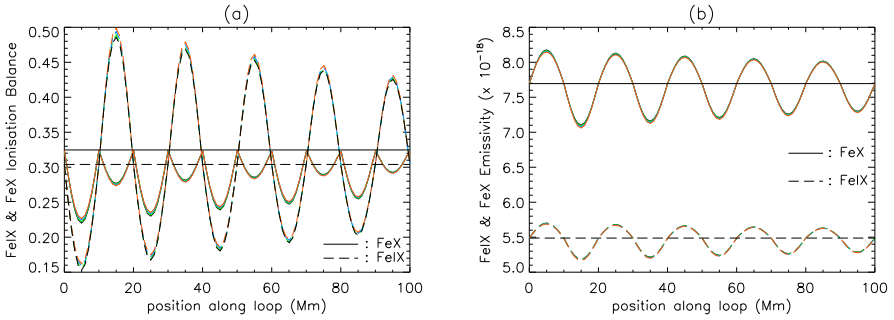

Figure 4. The scaled Fe IX (long-dashed lines) and Fe X (solid lines) ionisation balance (a) and emissivity (b) for the same perturbations as described in Figure 3. The horizontal lines represent the relevant background values.

Looking at the Fe X emissivity (Figure 4b), we can already see a slight asymmetry, with the minima being somewhat more pronounced than the maxima. However, the main reason for the very pronounced asymmetry in the Fe X emission is the ionisation balance of Fe X around $T_0 = 10^6$ K (Figure 4a), which never actually goes above its background value (solid horizontal line). Indeed, as the maximum of the Fe X ionisation balance occurs at $T_0 = 10^6$ K (see Figure 2a), both an increase and decrease in temperature will lead to a decrease in the ionisation balance. In fact, looking at Figure 4 (a) carefully, we can see that an increase in temperature actually causes a bigger decrease in the ionisation balance than a similar decrease in temperature, as expected from the steepness of the gradients in B_{FeX}. The combination of the slight asymmetry in the Fe X emissivity and the ionisation balance which is always below its background value leads to the suppression of the maxima in the Fe X emission and an enhancement of the minima, resulting in the very pronounced asymmetry seen in Figure 3.

Similarly, the behaviour of the Fe IX emission (Figure 3 (b) - long-dashed lines) can be understood by looking at the nature of the corresponding ionisation balance and emissivity (Figure 4 - long-dashed lines). The emissivity of Fe IX is somewhat smaller than Fe X but behaves largely in the same way. However, the Fe IX ionisation balance is actually 'reversed': an increase in temperature leads to a decrease in the ionisation balance and vice versa, as the background temperature of 1 MK is situated to the right of the peak of the Fe IX ionisation balance (i.e. the peak of the Fe IX ionisation balance occurs at a lower temperature - see Figure 2a). Around 1 MK, the amplitude of these 'inverse' perturbations in the ionisation balance is large enough to cause the same inverse behaviour in the Fe IX emission, as seen in Figure 3 (b).

For the larger perturbation amplitudes, the Fe IX emission maxima (which actually occur when the temperature and density reach a minimum) start to 'dip' (see Figure 3b - long-dashed lines). The perturbation amplitude at which these turn-arounds first start to occur can be predicted by considering when the emission reaches a maximum (i.e. $I'_{FeIX} = 0$) for $\delta T \neq 0$ and $\delta n \neq 0$. For a full derivation, we refer the reader to the Appendix. However, only considering the perturbations to the ionisation balance and density (ignoring the

emissivity) gives a good qualitative approximation, in the sense that it is a good approximation to the *behaviour* of the Fe IX emission, not to its actual value. To avoid any confusion, we will denote this 'approximation' as $\tilde{I}_{FeIX}$, where $\tilde{I}_{FeIX} = n_0^2 B_0 (1+\delta n)^2 (1+c\delta T)$, and hence, using $\delta n = \delta T/(\gamma-1)$,

$$\begin{aligned}
\tilde{I}'_{FeIX} &= 2\left(1+\frac{\delta T}{\gamma-1}\right)\frac{\delta T'}{\gamma-1}(1+c\delta T) + \left(1+\frac{\delta T}{\gamma-1}\right)^2 c\delta T' = 0 \\
&\Leftrightarrow \frac{2}{\gamma-1}(1+c\delta T) + c\left(1+\frac{\delta T}{\gamma-1}\right) = 0 \\
&\Leftrightarrow \delta T = -\frac{c(\gamma-1)+2}{3c}\,. \qquad (8)
\end{aligned}$$

For values less than $T_0 = 10^6$ K (remember, the maxima of B_{FeIX} occur as T is *de*creasing), a linear fit to the Fe IX ionisation balance gives a gradient $c = -4.77$, leading to $\delta T = 8.3\%$. However, this is the value of δT close to the first minimum of the temperature along the loop. The corresponding initial perturbation amplitude can be found by considering $\delta T \approx 8.3/\exp(-\alpha\frac{3\pi}{2}\frac{0.2}{2\pi}) = 8.8\%$. Hence, for perturbations larger than about 8.8% around $T_0 = 10^6$ K, we can expect the Fe IX emission to exhibit these dipped maxima. The full calculation given in the Appendix leads to a perturbation amplitude $\delta T \approx 6.3\%$.

Although we have only investigated the behaviour of the synthesised TRACE 171 Å intensity in detail for one specific case, namely perturbations around $T_0 = 10^6$ K and $n_0 = 10^9$ cm^{-3}, the other examples in Table 2 can be analysed in a similar way. Basically, the interactions between the density, ionisation balance and emissivity of Fe IX and Fe X are highly non-linear, making the relation between the input density and temperature perturbations and the resulting TRACE 171 Å intensity perturbations non-trivial. We remind the reader again that there is probably an additional effect due to the instrument response function but that this, for simplicity, has been absorbed into the emissivity E.

3.1.3. Altered Damping Profile

As pointed out in the discussion of Figure 1, the correct damping rate can be recovered in some cases, if the background intensity is known. However, this is not always the case. Let us for example consider perturbations around a background temperature of $T_0 = 0.95$ MK, with the temperature perturbation amplitude $\delta T = 10\%$, as shown in Figure 5 (a). Overplotted are the actual envelope of the perturbations (dashed line) and the original $e^{-\alpha z}$, with $\alpha = 0.5$, damping profile (dot-dashed lines). Note that the perturbation envelope (dashed lines) was obtained from the forward modelling code, not from fitting the maxima and minima of the perturbations. Clearly the (original) exponential damping profile has not survived the forward modelling process and, even knowing the background intensity, would not have been recovered from the 'observed' intensity perturbations. As the background temperature is still relatively high, the Fe X emission is again the dominant component of the synthesised TRACE 171 Å intensity. Looking at the Fe X ionisation balance (Figure 5b - solid lines), the reason for the altered damping profile becomes clear: although the background

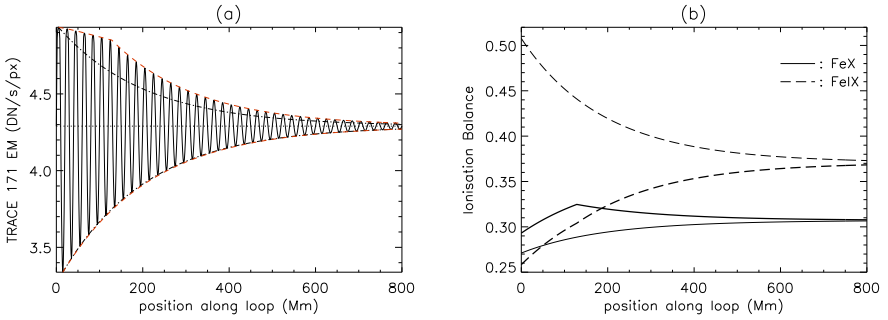

Figure 5. (a) TRACE 171 Å synthesised emission for a background temperature $T_0 = 0.95$ MK and a 10% perturbation ($\delta T = 0.1$). The actual envelope of the perturbations is outlined by the dashed line, where the dot-dashed line represents the original exponential damping profile. (b) The envelopes of the corresponding Fe IX (long dashed) and Fe X (solid line) ionisation balance. Thin and thick lines are the envelopes corresponding to the temperature (and density) minima and maxima, respectively.

temperature of $T_0 = 0.95$ MK is situated below the peak temperature of the Fe X ionisation balance ($T = 1$ MK), the initial perturbations in temperature are sufficiently large to reach values above this peak temperature (see Figure 2a). Hence, for the first few peaks of the perturbation, the Fe X ionisation balance actually has a negative gradient, only returning to the positive gradient when the temperature perturbations remain below 1 MK. Note that the Fe IX ionisation balance is again reversed (Figure 5b - long-dashed lines), with the ionisation balance decreasing for an increasing temperature and density and vice versa.

Finally, we briefly mention the example with $T_0 = 0.9$ MK and $\delta T = 15\%$. In this particular case, fitting the maxima along the first 100 Mm along the loop resulted not only in a different damping rate, but in an entirely different damping profile of $e^{-0.6\alpha z^3}$. Such a z^3-damping profile is a well-known characteristic of damping by phase mixing (see e.g. Heyvaerts and Priest, 1983), highlighting the need for a very careful interpretation of observed (intensity) damping rates as this 'observed' intensity perturbation could easily (*but wrongly!*) be interpreted as evidence of phase mixing of MHD waves in the solar corona.

3.2. TRACE and EIS 195 Å Intensity

We have repeated the determination of the damping rates for both the (synthesised) TRACE 195 Å and the EIS Fe XII (195.12 Å) emission, with background temperatures $T_0 = 1.4$ MK, $T_0 = 1.5$ MK and $T_0 = 1.6$ MK. The results are summarised in Table 2. For the TRACE 195 Å emission, both the Fe VIII and Fe XII were included but for the background temperatures considered in this analysis, the contribution of Fe VIII is negligible. This is clear from the results in Table 2, as both the synthesised TRACE 195 Å and EIS Fe XII emission give exactly the same estimated damping rates. As we really only have to take into account one emission line (Fe XII), the results for the 195 Å emission are somewhat easier to understand. However, the main conclusion remains the same, namely that the non-linear interactions between the density, ionisation balance

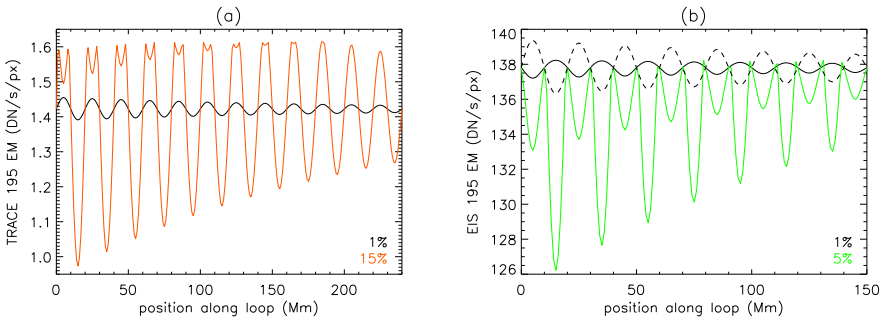

Figure 6. (a) TRACE 195 Å synthesised emission for a background temperature $T_0 = 1.5$ MK and a 1% (black) and 15% (red) perturbation. (b) EIS Fe XII (195.12 Å) synthesised emission for a background temperature $T_0 = 1.6$ MK and a 1% (black) and 5% (green) perturbation. Overplotted for comparison is the (scaled) temperature along the loop (dashed line).

and emissivity result in non-trivial, non-linear intensity perturbations. As the damping rates for the $T_0 = 1.4$ MK background temperature show no unexpected behaviour, we will not discuss these results in detail. Qualitatively, the TRACE and EIS synthesised emission behave identically and hence, we focus on one example of the TRACE 195 Å emission (with $T_0 = 1.5$ MK - Figure 6a), and one of the EIS Fe XII emission ($T_0 = 1.6$ MK - Figure 6b). Comparing the scaling of the vertical axes of both plots in Figure 6, the much higher sensitivity of the EIS detector is clearly apparent.

In Table 2, we can see that for $T_0 = 1.5$ MK and perturbation amplitudes of $\delta T = 1\%$ (Figure 6a - black line) and $\delta T = 5\%$ (not shown), the estimated damping rates of the intensity perturbations match the input damping rate rather well. However, as the amplitude of the perturbations gets larger, the maxima of the intensity are again suppressed. This can clearly be seen for the 15% perturbation (Figure 6a - red line), where the initial intensity maxima are actually increasing, before starting to decay further along the loop. Only looking at the first 100 Mm along the loop, resulted in the negative fraction (-0.2) given in Table 2 for this particular case (in other words, an $e^{0.2\alpha z}$ growth rate would have been found from observations, rather than the original $e^{-\alpha z}$ damping rate). The suppression of the maxima is largely caused by the Fe XII ionisation balance (solid line in Figure 2b): the behaviour of the ionisation balance is again reversed (increase in T, decrease in B_{FeXII}), where this decrease becomes much stronger for temperature perturbations larger than about 5.5%, due to the sharp change in the gradient of the ionisation balance. It is this enhanced decrease in the ionisation balance (occuring at the first few maxima in the temperature and density) which causes the suppression of the intensity maxima seen in Figure 6 (a) - red line.

Figure 6 (b) shows the synthesised EIS Fe XII emission for $T_0 = 1.6$ MK, with $\delta T = 1\%$ (black) and $\delta T = 5\%$ (green). Also shown, for comparison, is the corresponding (1%) temperature perturbation along the loop (dashed line). Note that this temperature has been scaled to fit on the same graph and hence that the values on the y-axis do not apply to this particular line. Two things are

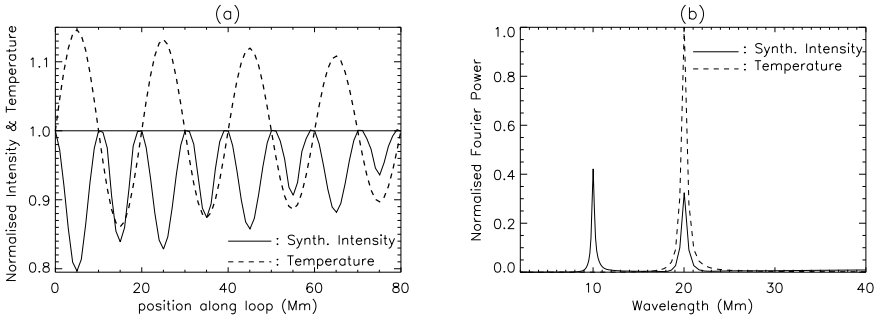

Figure 7. (a) Normalised TRACE 171 Å (synthesised) emission for a background temperature $T_0 = 1.1$ MK and a 15% perturbation ($\delta T = 0.15$). Overplotted (dashed line) is the corresponding (normalised) temperature along the loop. The horizontal line represents the background value of the 171 Å emission. (b) Fourier transform of both the TRACE 171 Å emission (solid line) and the temperature (dashed line).

immediately obvious, namely that the 1% intensity oscillations are out of phase with the input temperature (and density) and secondly, that the 5% intensity behaves very differently. The reversal in phase again reflects the behaviour of the Fe XII ionisation balance, where the 'reversed' perturbations in the ionisation balance are now large enough to dominate the Fe XII emission. For the larger amplitude perturbations, the situation is somewhat more complicated. Here, the (scaled) maxima in the ionisation balance (occuring at minima of T) are smaller than for the 1% pertubation, whereas the corresponding minima in the emissivity (also at minima of T) are more pronounced. The combination of both the smaller maxima in B and more pronounced minima in E means that the resulting Fe XII emission shows a very pronounced minimum. Put simply, at the maxima in T, there is a large dip in B and only a small peak in E, leading to dips in the Fe XII emission. On the other hand, at the minima of T, the maxima of B are less pronounced, whereas the dips in E are relatively large, again giving (even larger) dips in the Fe XII emission. Hence, in this particular case ($T_0 = 1.6$ MK and δT larger than a few percent), the Fe XII emission never actually goes above its background value, resulting in the very asymmetric behaviour seen in Figure 6 (b) - green line.

4. Effect on Periodicity

In a few of the examples discussed so far, we have come across 'dipped' maxima in the intensity perturbations. Looking at e.g. Figure 6b (green line), it is not hard to imagine that there might be cases where the dips in the maxima are so great that they actually become minima, leading to an apparent change in the periodicity. One such example is given in Figure 7 (a), which shows the (normalised) TRACE 171 Å intensity perturbations (solid line) and temperature (dashed line) for a background temperature of 1.1 MK and a 15% perturbation ($\delta T = 0.15$). Because we are working with analytical examples, we know the background value of the intensity (horizontal line), making it relatively easy

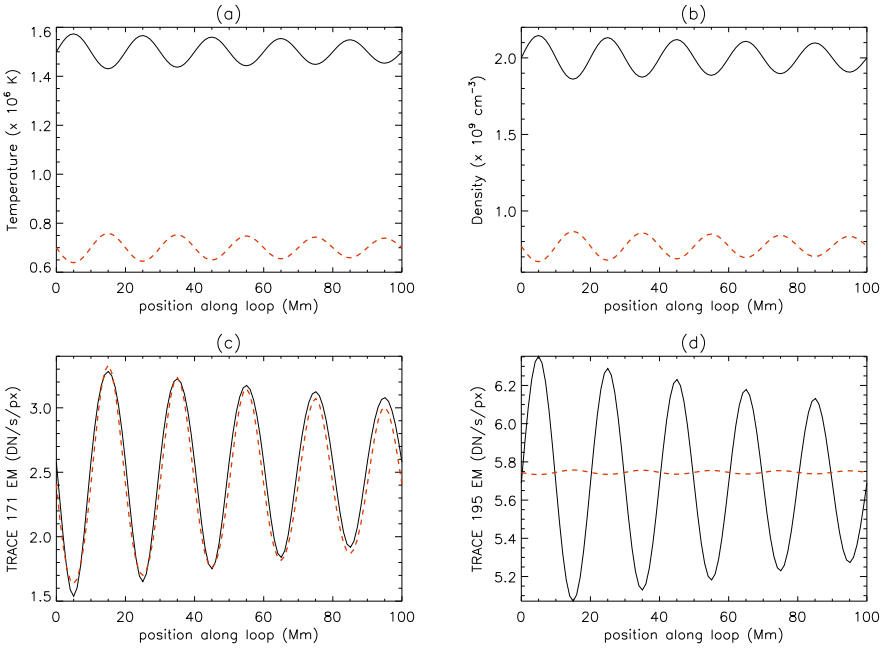

Figure 8. (a) Temperature, (b) density, (c) synthesised TRACE 171 Å and (d) TRACE 195 Å emission for 2 different sets of perturbations: solid lines - $T_0 = 1.5 \times 10^6$ K, $n_0 = 2 \times 10^9$ cm^{-3}, $\delta T = 5\%$, $\phi_T = \phi_0 = 0$; dashed lines - $T_0 = 0.7 \times 10^6$ K, $n_0 = 0.77 \times 10^9$ cm^{-3}, $\delta T = 9\%$, $\phi_T = \phi_0 = \pi$. An arbitrary value of 5.7 was added to the dashed 195 Å intensity.

to recognise the strongly dipped maxima, as the synthesised intensity always remains below the background value. However, to the 'real' observer, this would probably appear as an intensity oscillation around a (normalised) background value of about 0.95, especially if a reduced sampling rate makes the exact size of the extreme somewhat less clear. More importantly, the 'reversed' maxima give the intensity oscillation a different wavelength (or periodicity). Indeed, the corresponding Fourier transforms (Figure 7b) show a single peak at a wavelength of 20 Mm for the temperature (dashed line), but an additional peak at half that wavelength for the intensity (solid line). In this particular case, the power of this second peak is only slightly larger and the presence of two peaks of similar amplitude in the Fourier spectrum could have been interpreted as evidence for higher harmonics.

5. Ill-Posed Problem

The complex interactions between the density, ionisation balance and emissivity (possibly of several different elements) naturally lead to the question of the uniqueness: could different combinations of temperature and density perturbations actually lead to the same (observed) intensity? Unfortunately, the answer to this question is yes, implying that the problem is ill-posed. Figure 8 shows

two different sets of temperature (Figure 8a) and density (Figure 8b) which result in extremely similar synthesised TRACE 171 Å emission (Figure 8c) over the first few cycles of the perturbation. For the first set (solid lines), we used a relatively high background temperature of $T_0 = 1.5$ MK, a background density $n_0 = 2 \times 10^9$ cm^{-3} and a (temperature) perturbation amplitude of 5%. Other parameters were as before, with perturbations in temperature and density still related by $\delta n = \delta T/(\gamma - 1)$. On the other hand, the dashed lines correspond to a much cooler background temperature $T_0 = 0.7$ MK, $n_0 = 0.77 \times 10^9$ cm^{-3} and $\delta T = 9\%$. The phase of these perturbations was reversed by setting $\phi_T = \phi_0 = \pi$.

Looking at the first 100 Mm along the loop, the TRACE 171 Å intensity (Figure 8c) corresponding to these different sets of input parameters is virtually indistinguishable, especially if one keeps in mind that real observations would probably have a reduced sampling rate (resolution) and would suffer from additional noise. Around about 80-100 Mm along the loop, one can just about see that the intensities will tend to different background values, with the lower temperature intensity tending to a slightly lower value. However, the difference between these background values was very small ($\sim$2.4 vs $\sim$2.6 DN pixel^{-1} s^{-1}). Note that for the higher background temperature (solid lines), the TRACE 171 Å intensity is actually out of phase with the input temperature and density perturbations. One possible way to distinguish the two different sets is to look at observations made with a different filter or emission line. As an example, the corresponding TRACE 195 Å intensity is shown in Figure 8 (d), where an arbitrary value of 5.7 was added to the lower temperature intensity (dashed line), to be able to represent both curves on the same graph. Not unexpectedly, the synthesised TRACE 195 Å emission corresponding to the lower temperature is totally negligible, keeping in mind the size of this arbitrary constant. Note also that in both cases, the 195 Å intensity is in phase with the associated temperature and density perturbations.

The example presented in this section was chosen at random and does not represent an isolated case. A thorough search through the relevant parameter space is likely to result in many combinations that lead to very similar intensities, for any chosen instrument filter or emission line.

6. Discussion and Conclusions

In this paper, we have demonstrated with some selected examples, relevant to the solar corona, that the nature of the (input) temperature and density perturbations does not necessarily 'survive' the forward modelling. Both the damping rate and profile, as well as the phase of the oscillations can change and in some, more extreme cases, it is possible that even the wavelength (period) is modified. This does not, in any way, reflect on the quality of the chosen instrument or emission lines. The TRACE instrument was simply chosen because it is a well known and widely used imager, whereas the EIS Fe XII (195.12 Å) was included to be able to compare with a spectrometer. These results do however emphasise the need to include forward modelling when comparing theoretical models with observed intensity oscillations, even for a basic, qualitative comparison, as one cannot

assume that the observed intensity perturbations will necessarily behave in the same way as the (model) temperature and density. Our results are especially relevant for the rapidly developing subject of coronal seismology (De Moortel, 2005), which, by its very nature, relies heavily on the (*correct!*) interpretation of properties such as damping rate and phase of observed intensity oscillations, very often (although not exclusively) from imaging instruments such as TRACE.

The main reason for this non-trivial relation between temperature and density on the one hand, and observed intensity on the other hand, is the complex, non-linear interaction between the individual components which make up the emission: density (squared), ionisation balance and emissivity (and the instrument response function). Generally, the emissivity is well behaved, with an oscillatory pattern resembling the input temperature and density (in the sense that the perturbations in the emissivity have the same periodicity and are in phase with T and n). The oscillatory behaviour of the ionisation balance, however, often shows a very different pattern, depending on where the background temperature is situated in relation to the peak temperature of the relevant ionisation balance. Hence, the perturbations in the ionisation balance can be 'reversed', where the ionisation balance decreases when T increases and vice versa, or have suppressed or even 'dipped' maxima, where these dips can sometimes be so extreme, that the ionisation balance never actually goes above its background value.

The implications of a modified damping rate or profile are extremely important when trying to identify the underlying dissipation mechanism on the basis of the observed damping. As some wave damping mechanisms exhibit a characteristic damping profile (e.g. the z^3-profile of phase mixing), the modification of this profile (i.e. the fact that the observed intensity does not necessarily have the same profile as the underlying temperature and/or density) could lead to an entirely wrong conclusion about the dominant damping mechanism. Similarly, the change in phase that was found in some cases, where the resulting intensity perturbations are out of phase with the input temperature and density, could strongly affect travel time calculations. Indeed, these calculations are based on estimating phase differences between intensity oscillations observed in different emission lines (and hence at different heights) and therefore, it is crucial to know that there is no change in phase just because, say, the behaviour of the ionisation balance of a particular emission line. The modification of the properties of the periodic disturbances presented in this paper is reminiscent of the results of Parenti et al. (2006), who found that the power-law index of an input energy distribution was not conserved in the synthesised emission.

The results of Section 5 demonstrated that the problem can be ill-posed: different combinations of input temperature and density can result in almost identical intensity observed in a particular passband or emission line (see also Wikstol, Judge and Hansteen (1998), Judge and McIntosh (1999) or McIntosh (2000) and references therein). However, this will almost certainly only occur in that particular passband, and a comparison with observations in a different passband or emission line should go a long way in resolving any ambiguity. The fact that both the TRACE 195 Å and EIS Fe XII (195.12 Å) emission produce identical 'results' is interesting in its own right, demonstrating that

stand-alone line-integrated spectroscopic (intensity) observations do not offer a clear advantage over imaging observations. However, in practise, it is likely that the spectroscopic observations would consist of a multitude of emission lines observed simultaneously, which will certainly be useful when trying to disentangle the various issues mentioned above. Any (spectroscopic) information on Doppler shifts will be an added bonus. The results did however nicely highlight the greatly improved sensitivity of the EIS detector.

The study presented in this paper is not intended to model any specific physical or dynamical processes occurring in the solar atmosphere. Our purpose was solely to demonstrate that one cannot necessarily assume a one-to-one relation between observed (or synthesised) intensity oscillations and the associated temperature and density perturbations (in terms of which theoretical models are often expressed). To keep our analysis simple, we made a number of assumptions which could be improved upon in a more detailed treatment of a specific problem. Most importantly, the assumption of ionisation equilibrium is only valid when considering perturbations on timescales relatively long compared to the ionisation and recombination rates of the relevant ions. For Fe ions in a coronal environment ($T \sim 10^6$ K - $n \sim 10^9$ cm^{-3}), the timescale for the Fe X and Fe XII populations to equilibrate is of the order of a few to tens of seconds, sufficiently short to warrant the assumption of ionisation equilibrium when considering perturbations in temperature and density on timescales of a few minutes. Furthermore, the relation between the temperature and density perturbations we have used in this analysis ($\delta n = \delta T/(\gamma - 1)$) is based on the adiabatic MHD equations. Non-adiabatic processes such as thermal conduction or optically thin radiation will modify the relative size of the temperature and density perturbations and could even affect the phase. Furthermore, we have only used linear interpolation to determine the appropriate ionisation balance and emissivity from the look-up tables. Finally, we note that we only considered the dominant emission lines in the calculations of the TRACE synthesised emission (171 Å: Fe IX and Fe X - 195 Å: Fe VIII and Fe XII). However, for the range of temperatures and densities considered in this paper, this is likely to be sufficient.

To conclude: we have shown that observational data from imagers and line-integrated intensities from spectrometers alike are subject to misinterpretation due to the non-linear interactions between the parameters that govern the formation (emissivity, ionisation balance) and measurement (instrument response function) of emission lines. Forward-modelling provides a way to guard against the misinterpretation of observational data by allowing one to synthesise the likely observational characteristics of a particular event and, with apriori knowledge of the event, determine how accurately one may have recovered the underlying physics of the event from the observational data alone.

Acknowledgements: IDM and SB acknowledge support of a Royal Society University Research Fellowship and STFC Postdoctoral Fellowship, respectively. The authors would also like to thank Profs. A.W. Hood and P.J. Cargill for many useful discussions.

Appendix

We reconsider the calculation of the 'dipped' maxima in the Fe IX emission for perturbations around $T_0 = 10^6$ K, using the full expression for I_{FeIX}:

$$I_{FeIX} = n_0^2(1+\delta n)^2 \times B_0(1+c\delta T) \times E_0(1+a\delta n + b\delta T)\,.$$

In order to find when the turn-around in the Fe IX emission occurs, we need to determine when $I'_{FeIX} = 0$ for $\delta T \neq 0$ and $\delta n \neq 0$. Using the above expression for the Fe IX emission, I'_{FeIX} is given by

$$\begin{aligned} I'_{FeIX} = \quad & n_0^2\, B_0\, E_0\, [2(1+\delta n)\delta n'(1+c\delta T)(1+a\delta n + b\delta T) \\ & +(1+\delta n)^2 c\delta T'(1+a\delta n + b\delta T) \\ & +(1+\delta n)^2(1+c\delta T)(a\delta n' + b\delta T')]\ . \end{aligned}$$

Setting $\delta n = \delta T/(\gamma-1)$ and (for convenience of notation) $A = a/(\gamma-1)+b$, we find

$$\begin{aligned} & I'_{FeIX} = 0 \\ & \Rightarrow 2\left(1+\frac{\delta T}{\gamma-1}\right)\frac{\delta T'}{\gamma-1}(1+c\delta T)(1+A\delta T) + \left(1+\frac{\delta T}{\gamma-1}\right)^2 c\delta T'(1+A\delta T) \\ & \qquad\qquad + \left(1+\frac{\delta T}{\gamma-1}\right)^2 (1+c\delta T)A\delta T' = 0 \\ & \Rightarrow 4Ac\delta T^2 + [3c+2A+2Ac(\gamma-1)]\delta T + (A+c)(\gamma-1)+2 = 0 \\ & \Rightarrow \delta T = \frac{-(3c+2A+2Ac(\gamma-1))}{8Ac} \\ & \qquad\qquad \pm\frac{\sqrt{(3c+2A+2Ac(\gamma-1))^2 - 16Ac[(A+c)(\gamma-1)+2]}}{8Ac}\,. \end{aligned}$$

Just below $T_0 = 10^6$ K, we find $a = 0$, $b = 0.44$ and $c = -4.77$, giving $\delta T = 5.8\%$ at the first minimum and hence, an original (i.e. at $z = 0$) temperature perturbation of $\delta T \approx 5.8/\exp(-\alpha\frac{3\pi}{2}\frac{0.2}{2\pi}) = 6.3\%$.

References

Aiouaz, T., Peter, H., Keppens, R.: 2005, *Astron. Astrophys.* **442**, L35.
Bradshaw, S.J., Mason, H.E.: 2003a, *Astron. Astrophys.* **401**, 699.
Bradshaw, S.J., Mason, H.E.: 2003b, *Astron. Astrophys.* **407**, 1127.
Bradshaw, S.J., Cargill, P.J.: 2006, *Astron. Astrophys.* **458**, 987.
Cargill, P.J.: 1993, *Solar Phys.* **147**, 263.
Cargill, P.J.: 1994, *Astrophys. J.* **422**, 381.
Cargill, P.J., Klimchuk, J.A.: 1997, *Astrophys. J.* **478**, 799.
Cargill, P.J., Klimchuk, J.A.: 2004, *Astrophys. J.* **605**, 911.
Culhane, J.L. et al.: 2007, *Solar Phys.* **243**, 19.

De Groof, A., Berghmans, D., van Driel-Gesztelyi, L., Poedts, S.: 2004, *Astron. Astrophys.* **415**, 1141.
De Moortel, I.: 2005, *Roy. Soc. Phil. Trans. A* **363**, 2743.
Dere, K.P., Landi, E., Mason, H.E., Monsignori Fossi, B.C., Young, P.R.: 1997, *Astron. Astrophys. Suppl. Ser.* **125**, 149.
Feldman, U., Mandelbaum, P., Seely, J.L., Doschek, G.A., Gursky H.: 1992, *Astrophys. J. Suppl. Ser.* **81**, 387.
Gudiksen, B.V., Nordlund, A.: 2005, *Astrophys. J.* **618**, 1020.
Handy, B.N. et al.: 1999, *Solar Phys.* **187**, 229.
Hansteen, V.H.: 1993, *Astrophys. J.* **402**, 741.
Heyvaerts, J., Priest, E.R.: 1983, *Astron. Astrophys.* **117**, 220.
Innes, D.E., Tóth, G.: 1999, *Solar Phys.* **185**, 127.
Judge, P.G., McIntosh, S.W.: 1999, *Solar Phys.* **190**, 331.
Klimchuk, J.A., Cargill, P.J.: 2001, *Astrophys. J.* **553**, 440.
Lundquist, L.L., Fisher, G.H., McTiernan, J.M., Régnier, S.: 2004, ESA-SP **575**, 306.
Mazzotta, P., Mazzitelli, G., Colafrancesco, S., Vittorio, N.: 1998, *Astrophys. J.* **133**, 403.
McIntosh, S.W.: 2000, *Astrophys. J.* **533**, 1043.
Müller, D., Peter, H., Hansteen, V.H.: 2004, *Astron. Astrophys.* **424**, 289.
Müller, D., De Groof, A., Hansteen, V.H., Peter, H.: 2005, *Astron. Astrophys.* **436**, 1067.
Nakariakov, V. M., Verwichte, E.: 2005, *Living Rev. Solar Phys.* **2**, 3 (http://www.livingreviews.org/lrsp-2005-3).
Parenti, S., Buchlin, E., Cargill, P.J., Galtier, S., Vial, J.-C.: 2006, *Astrophys. J.* **651**, 1219.
Peter, H., Gudiksen, B.V., Nordlund, A.: 2004, *Astrophys. J.* **617**, L85.
Peter, H., Gudiksen, B.V., Nordlund, A.: 2006, *Astrophys. J.* **638**, 1068.
Sarro, L.M., Erdélyi, R., Doyle, J.G., Pérez, M.E.: 1999, *Astron. Astrophys.* **351**, 721.
Taroyan, Y., Bradshaw, S.J., Doyle, J.G.: 2006, *Astron. Astrophys.* **446**, 315.
Taroyan, Y., Erdélyi, R., Wang, T.J., Bradshaw, S.J.: 2007, *Astrophys. J.* **659**, L173.
Wikstol, O., Judge, P.G., Hansteen, V.H.: 1998, *Astrophys. J.* **501**, 895.
Young, P.R., Del Zanna, G., Landi, E., Dere, K.P., Mason, H.E., Landini, M.: 2003, *Astron. Astrophys. Suppl. Ser.* **144**, 135.